phys. stat. sol. (a) **205**, No. 7, 1705–1712 (2008) / **DOI** 10.1002/pssa.200723403

physica status solidi a
www.pss-a.com
applications and materials science

# Improved quality nonpolar *a*-plane GaN/AlGaN UV LEDs grown with sidewall lateral epitaxial overgrowth (SLEO)

**Bilge Imer[*,1], Matt Schmidt[1], Ben Haskell[1], Siddharth Rajan[2], Barry Zhong[1], Kwangchoong Kim[1], Feng Wu[1], Tom Mates[1], Stacia Keller[2], Umesh K. Mishra[2], Shuji Nakamura[1,2], James S. Speck[1], and Steven P. DenBaars[1,2]**

[1] University of California Santa Barbara, Materials Department, Santa Barbara, CA 93106, USA
[2] University of California Santa Barbara, Electrical & Computer Engineering Department, Santa Barbara, CA 93106, USA

Received 31 August 2007, revised 11 February 2008, accepted 14 February 2008
Published online 28 May 2008

**PACS** 78.60.Fi, 81.05.Ea, 81.15.Gh, 85.60.Jb

[*] Corresponding author: e-mail bilge@engineering.ucsb.edu

High quality nonpolar *a*-plane GaN templates were grown by utilizing sidewall lateral epitaxial overgrowth (SLEO) technique with threading dislocation density of $\sim 10^6$–$10^7$ cm$^{-2}$. 360 nm GaN/AlGaN multiple quantum well ultraviolet light emitting diodes were grown with metalorganic chemical vapor deposition. Reduced defect density SLEO *a*-plane, planar *a*-plane, and planar *c*-plane templates were co-loaded for device growth and processed together in order to make relative device performance comparison. For SLEO *a*-plane LEDs EL peak position was measured at 360 nm and it was independent of drive current. The linewidth of the emission was 7 nm. The series resistance of these diodes was as low as 16.5 Ω and the forward voltage was measured as 4.08 V at 20 mA. The external quantum efficiency of the high quality SLEO *a*-plane devices was ~275× higher than planar *a*-plane devices. The highest output power was realized at 200 mA as 65 μW. The effect of contact geometry on electrical and optical characteristics of the devices was also discussed.



**1 Introduction** III-nitrides cover the entire visible, UV and infrared spectral region with the bandgap ranging from 0.65 eV to 6.2 eV. Possible use of GaN based UV devices include high density data storage, solid state lighting, and sensor applications. So far i-line (365 nm) Mercury lamps have been used as UV sources, but mercury is toxic and not environmentally friendly. Because of its nontoxicity, thermal and chemical stability, long lifetime and small size, GaN is the major potential substitute to operate at this wavelength range. However the external quantum efficiency (EQE) of these devices is still extremely poor, especially below 370 nm. The highest EQE for polar UV LEDs to date has been reported by Morita et al. [1] in 2004 as 44% at 365 nm with 1 A pulsed operation and 5% duty cycle. As the operation wavelength range gets shorter, the efficiencies start to suffer from defect densities, absorption, polarization and poor doping more. While highest EQE was reported as 4% for 343 nm UV LEDs operating at 20 mA [2], the EQE value dropped down to 0.07% for 247 nm LEDs with Al content over 70% operating at 90 mA [3]. Threading dislocations (TDs) act as nonradiative recombination centers leading to reduced internal quantum efficiencies [4], so defect reduction methods should be utilized to eliminate them. Most nitride-based LEDs rely on n-GaN buffer layers and p-GaN capping layers for good current spreading and low contact resistance. These layers absorb at 370 nm or lower wavelength [5]. Therefore reduced defect density wider bandgap templates such as AlGaN or AlN should be produced without cracking to prevent absorption; the templates with semipolar or nonpolar orientations should be employed to avoid polarization in order to improve upon device efficiencies in the UV range.

In the UV wavelength range, 370 nm and lower, as the bandgap gets wider the efficiencies start to suffer from defect densities, absorption, polarization and poor doping. For nonpolar III-Nitrides, these adverse effects are more pronounced due to higher defect densities, limited growth

windows, and not well understood doping behavior. Although there are some reports on EQE of nonpolar LEDs in the blue and violet range of the spectra [6, 7] and numerous studies reporting EQE of polar UV LEDs at 365 nm [1–3], there is no report on EQE of nonpolar UV LEDs because of poor crystal quality and high defect densities of these nonpolar films (TDs ~$10^{10}$ cm$^{-2}$) [8, 9]. In 2003 Chen et al. reported the first *a*-plane GaN/AlGaN 363 nm UV LEDs with high series resistance (65 Ω) and turn-on voltage of 4 V [10] but there was not any information on EQE of these devices. Morita et al. [1] proved that below TD value of $10^8$ cm$^{-2}$ high-efficiency UV LEDs are possible to accomplish. At this point two of the so-called challenges have been surmounted by growing high quality reduced defect density (TDs ~$10^6$–$10^7$ cm$^{-2}$ throughout the material) nonpolar *a*-plane GaN templates with the sidewall lateral epitaxial overgrowth (SLEO) method [11]. In this paper, device performance of 360 nm GaN/$Al_{0.15}$GaN UV LEDs grown on SLEO material is discussed in detail and compared with planar *a*- and planar *c*-plane GaN LEDs.

In polar GaN/AlGaN QWs, the separation of the wavefunctions due to the built-in electric field induces long radiative lifetime, which in turn leads to a charge accumulation in the wells. The effects of charge accumulation is only partially compensated by the nonradiative recombination channels and it becomes increasingly important in wider wells, in which the separation of the wavefunctions is larger [12]. Therefore in active region the well and the barrier width become extremely important in influencing the quantum efficiencies. If the wells are too thin (<2 nm for polar *c*-plane GaN), the efficiency decreases due to enhanced carrier leakage to the underlying layers. On the other hand if the wells are too thick (>4 nm for polar *c*-plane GaN), due to strain relaxation and defect formation, the efficiencies start to suffer from increased non-radiative recombination rate approaching the critical thickness of MQWs as well as a large red-shift due to the presence of strong piezoelectric field. Therefore the optimum well width for polar *c*-plane GaN QWs was determined to be 3 nm by several groups [13, 14]. In the case of nonpolar QWs, the transitions between conduction and valance bands occur with flat band conduction [15–17]. The wavelength does not shift with change in current. Therefore, well and/or barrier width only determines the intensity of the emission peak and the lifetimes of the carriers. 3 nm well width was also verified to be the optimum value for nonpolar *a*-plane GaN QWs [17].

In order to compare defective planar films and reduced defect density films, and to make comparative analysis between polar versus nonpolar films, nonpolar SLEO *a*-plane GaN, nonpolar planar *a*-plane GaN, and polar planar *c*-plane GaN films were co-loaded for device growth. A well width of 3 nm was chosen as it was determined to be the optimum well width to minimize polarization effects in polar films, and the highest intensity with the lowest radiative lifetimes were obtained because of better electron–hole wavefunction overlap in nonpolar *a*-plane GaN/AlGaN quantum wells. The barrier width of 10 nm was chosen with 15% Al content for good electrical confinement.

## 2 Experimental

**2.1 Device growth** The LED structures were grown on ~1.5 µm nonpolar planar *a*-plane GaN, ~1.5 µm polar planar *c*-plane GaN, and ~20 µm MOCVD initiated HVPE coalesced nonpolar SLEO *a*-plane GaN templates. The size of the LEO stripes were 5 µm/15 µm (window/wing) oriented along the m-direction as described in previous paper [11]. Planar *a*-plane GaN films had threading dislocation (TD) density of ~$2 \times 10^{10}$ cm$^{-2}$ and stacking fault (SF) density of ~$3.5 \times 10^5$ cm$^{-1}$. SLEO *a*-plane GaN films had threading dislocation (TD) density of ~$10^6$–$10^7$ cm$^{-2}$ and stacking fault (SF) density of ~$10^3$–$10^4$ cm$^{-1}$. And the planar *c*-plane GaN films had TD density of ~$10^7$–$10^8$ cm$^{-3}$. The device growth was carried out in a vertical close-spaced rotating disk 1 × 2″ Thomas Swan MOCVD reactor. The structure (from bottom to top) consisted of ~0.5 µm GaN:Si (~$2 \times 10^{19}$ cm$^{-3}$), 7 periods of GaN/$Al_{0.15}$GaN (3/10 nm) MQW active region, ~20 nm $Al_{0.2}$GaN barrier layer, ~200 nm $Al_{0.05}$GaN:Mg, and lastly, a ~20 nm heavily doped GaN contact layer. The device structure schematic is shown in Fig. 1.

**2.2 Device processing** Following the growth, devices were annealed for p-activation with rapid thermal annealing (RTA) in $N_2/O_2$ ambient at 700 °C for 15 minutes. The Pd/Au (50 Å/50 Å) p-metal contacts were patterned by lithography. A mesa etch in $Cl_2$ based reactive ion etching (RIE) was followed by Ti/Al/Au (200 Å/2000 Å/3500 Å) n-metal contact lithography. Processing was finalized with Ti/Au (200 Å/3000 Å) thick pad metal deposition.

**2.3 Device testing** There were three types of devices differing by their contact geometry; Interdigitated (E-shaped, or finger pattern), U-shaped, and L-shaped. The interdigitated contact geometry was proposed to prevent cur-

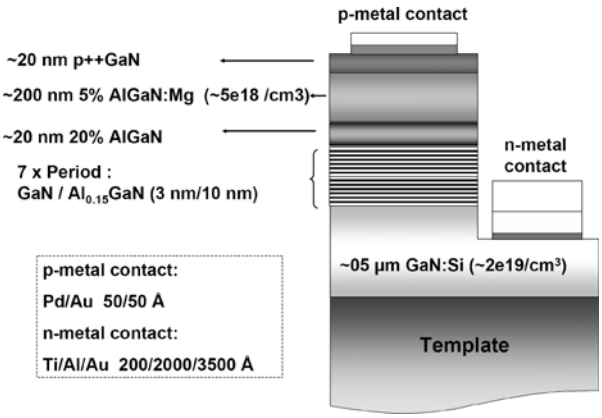


**Figure 1** GaN/$Al_{0.15}$GaN LED device structure and metal contacts used.

 

rent crowding and reduce the series resistance [18–20]. Each contact geometry, there were three sizes of junction areas with 300 × 300 μm, 400 × 400 μm, and 500 μm on the mask.

The devices were tested for $I$–$V$ and $E$–$L$ with DC at room temperature. The power measurements were done at room temperature on unpackaged (on-wafer) LEDs. These device testing techniques were utilized to see the effect of defect densities, the effect of polarization fields, and the effect of the contact geometry on device performances.

**3 Results** In order to be able to make a relative comparison between the planar films and the SLEO films, SLEO *a*-plane GaN (TDs ~$10^6$–$10^7$ cm$^{-2}$), planar *a*-plane GaN (TDs ~$10^{10}$ cm$^{-2}$) and *c*-plane GaN (TDs ~$10^7$–$10^8$ cm$^{-2}$) templates were co-loaded for device growth and processed together. There is still some room for improvement in internal efficiency since the device structure and doping levels for this LED set were not optimized. Therefore, rather than absolute values, the relative values garner more significance.

**3.1 Current–voltage ($I$–$V$)** Depending on the contact geometry and test area, the series resistance for polar planar *c*-plane, nonpolar planar *a*-plane and SLEO *a*-plane LEDs was in the range of 28–34 Ω, 40–45 Ω, and 15–22 Ω, respectively. The series resistance values were found to be directly proportional with the defect densities; as planar *a*-plane GaN had the highest TD density (~$10^{10}$ cm$^{-2}$), SLEO *a*-plane GaN had the lowest TD density (~$10^6$–$10^7$ cm$^{-2}$), and planar *c*-plane GaN TD density was slightly higher than SLEO *a*-plane GaN (~$10^7$–$10^8$ cm$^{-2}$). Accordingly, as shown in the combined $I$–$V$ curves (Fig. 2a), nonpolar planar films had the highest series resistance (42 Ω) indicating presence of high defect density, the reduced defect density SLEO LEDs had the lowest resistance value (16.5 Ω). Series resistance value for polar *c*-plane GaN LEDs fell in between these two values with 30 Ω.

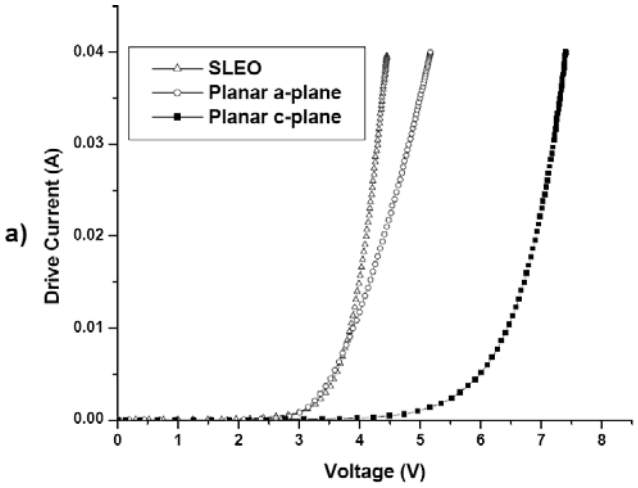


| Material | Series Resistance (Ω) | Turn-on Voltage (V) | Forward Voltage at I=20 mA (V) |
|---|---|---|---|
| SLEO a-plane | 16.5 | 3.75 | 4.08 |
| Planar a-plane | 42 | 3.55 | 4.4 |
| Planar c-plane | 30 | 6.3 | 6.9 |

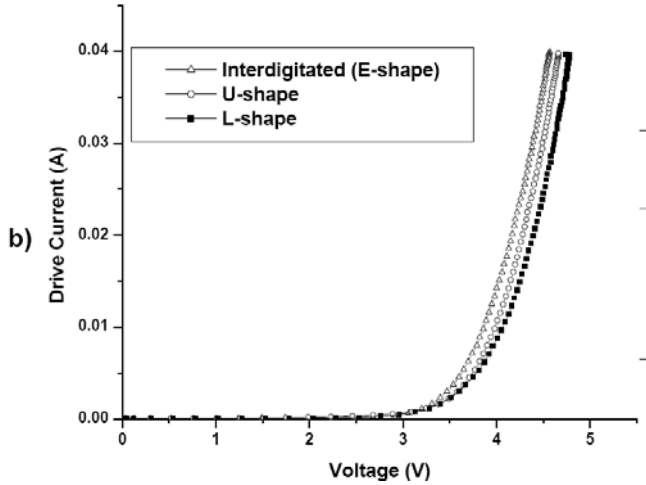


| Contact Geometry | Series Resistance (Ω) | Turn-on Voltage (V) | Forward Voltage at I=20 mA (V) |
|---|---|---|---|
| Interdigitated (E-shape) | 17.5 | 3.8 | 4.15 |
| U-shape | 20.5 | 3.85 | 4.25 |
| L-shape | 22.5 | 3.95 | 4.4 |

**Figure 2** Current–voltage characteristics for a) SLEO *a*-plane, planar *a*-plane, and planar *c*-plane LEDs with interdigitated contact geometry (400 × 400 μm junction area), and for b) interdigitated (E-shape), U-shape, and L-shape contact geometries on SLEO *a*-plane LEDs (400 × 400 μm junction area).

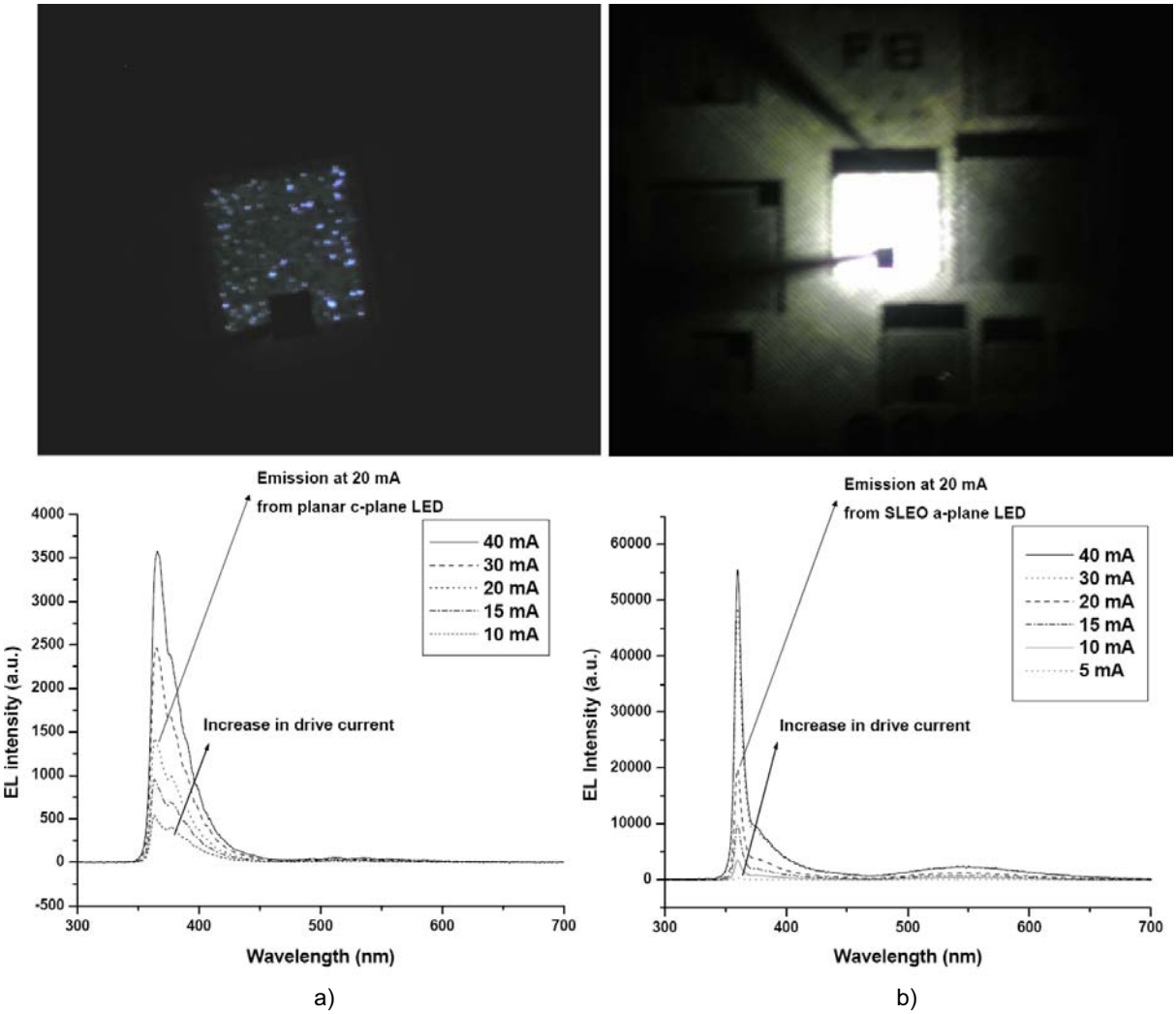


**Figure 3** (online colour at: www.pss-a.com) Change in EL spectra for change in currents (5–40 mA) and light emission at 20 mA bias from U-shape contact geometry a) planar *c*-plane GaN, and b) SLEO *a*-plane GaN on wafer LEDs under microscope (400 × 400 μm junction area).

Planar *c*-plane LED had turn-on voltage at ~6.3 eV, while nonpolar planar and SLEO *a*-plane LEDs turned-on at around 3.55 eV and 3.75 eV, respectively.

As shown in Fig. 2b, out of all devices from the same SLEO *a*-plane template, the interdigitated (E-shaped) contact geometry devices yielded the highest power, lowest forward voltage and lowest series resistance results due to better current spreading. Diode, contact and spreading resistance are the major contributors for series resistance. In this case, the material quality is the same and so is the internal resistance. However, since the contact geometry, contact and spreading resistances are different; they contribute differently in series resistance. Further discussion on effects of contact geometry is given in power measurement section later in this paper.

**3.2 Electroluminescence (EL)** All electroluminescence (EL) measurements were taken from unpackaged, on-wafer, LEDs. The light was extracted and collected from top. EL of the polar planar *c*-plane and nonpolar SLEO *a*-plane devices was measured at dc drive current in the range of 5–40 mA. The emission from planar *a*-plane GaN films was extremely weak which made capturing EL emission extremely hard. Although the *c*-plane GaN peak was measured at ~363 nm at 20 mA, the physical appearance of the light emission to naked eye was near violet due to combined effect of self-heating and intense broad self-absorption emission at ~370 nm. As shown in Fig. 3, due to the thermal effects, the *c*-plane GaN emission peak shifted from 363 nm to 366 nm as the drive current increased to 40 mA. The peak EL emission for nonpolar SLEO devices was at 360 nm and did not shift as the drive current increased from 5 mA to 40 mA, which indicates that the quantum well-band edge emission lacked polarization field effects and had better heat sinking capabilities due to underlying thick SLEO GaN template. From the same

 

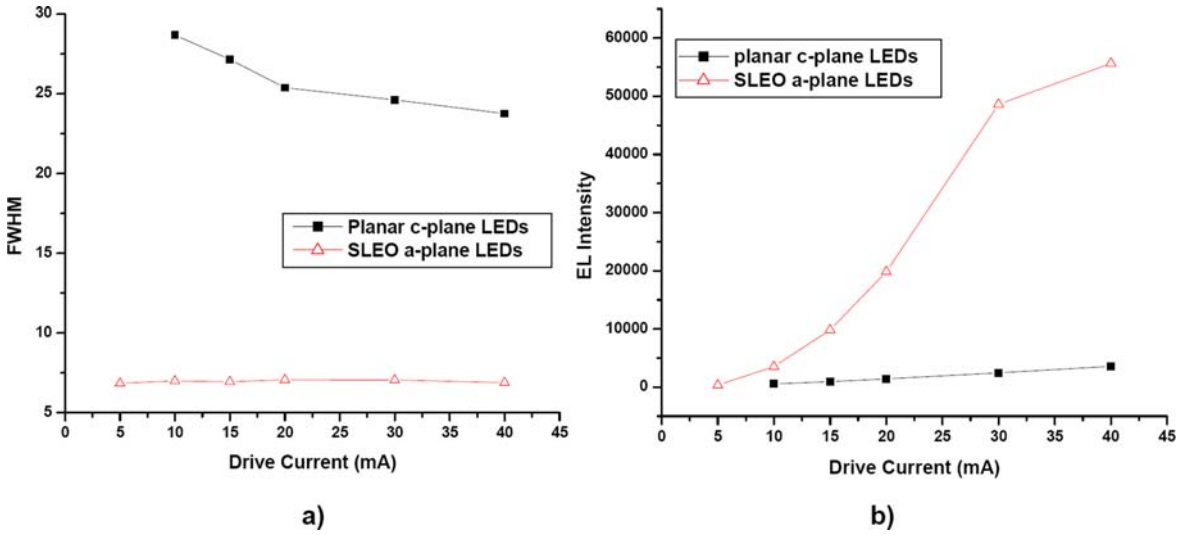


**Figure 4** (online colour at: www.pss-a.com) Comparison of change in a) EL FWHM, and b) EL intensity with increase in drive current for SLEO *a*-plane and planar *c*-plane LEDs (400 × 400 μm junction area).

figure, it was possible to see the difference in the homogeneity and intensity of the emission. As seen in Fig. 3b, nonpolar SLEO *a*-plane devices displayed distinct and homogeneous emission due to its low defect density (crystal quality) and low surface roughness values (Rms value of 0.6 nm for 20 μm × 20 μm atomic force microscopy (AFM) image), while polar planar *c*-plane LEDs exhibited inhomogeneous emission due to relatively larger variation in surface roughness values (Rms value of ~3 nm for 20 μm × 20 μm AFM image) and crystal quality (with slightly higher defect densities).

SLEO LEDs had 15 times higher peak intensity and 6 times less linewidth values. In EL spectra for both polar *c*-plane and nonpolar *a*-plane (Fig. 3), two other peaks were present other than GaN bandedge emission. One was deep yellow luminescence (YL) at ~2.2 eV and the other was emission at ~370 nm (~3.35 eV) which was associated with absorption of light in the underlying n-type GaN contact layers [21]. The self-absorption emission at 370 nm was in different shapes and intensity for SLEO *a*-plane GaN and planar *c*-plane GaN. This can be related to different GaN template thicknesses, presence of underlying $SiO_2$ mask in SLEO and relative luminous intensity of these two materials with respect to the absorption peak.

Figure 4 summarizes the FWHM and intensity values of planar *c*-plane and SLEO *a*-plane LEDs electroluminescence spectra. The typical linewidth value for SLEO *a*-plane device emission was 7 nm (Fig. 4a). With increase in drive current, FWHM did not get affected for SLEO devices, which also suggests that the device heating does not have a big impact due to the large film thickness and reduced internal resistance related with reduced defect density. However, for planar *c*-plane GaN FWHM value was in the range of 23–28 nm. It decreased with increase in drive current, which was the opposite of what was expected. This phenomenon was related with self-absorption emission at 370 nm. As the drive current increased, the bandgap emission intensity increased and with device heating wavelength shifted from 363 to 366 nm, getting closer to the 370 nm emission peak. As the two peaks, 370 nm absorption peak and 363 nm GaN emission peak, approached each other FWHM values decreased. Therefore, this trend in FWHM was the combined effect of wavelength shift and relative intensity of bandgap emission versus self-absorption emission and cannot be solely related to heat dissipation.

**3.3 Power and external quantum efficiency (EQE)** After testing over 200 SLEO *a*-plane GaN, 100 planar *c*-plane GaN, and 100 planar *a*-plane GaN LEDs, the power density results varied for planar *a*-plane GaN LEDs in the range of 0.02–0.05 μW; for planar *c*-plane GaN LEDs between 0.3–0.5 μW (10 times higher) and for the SLEO *a*-plane GaN in the range of 2.5–6.5 μW (100 times higher than planar *a*-plane GaN and 10 times higher planar *c*-plane GaN) at 20 mA drive current depending on the contact geometry.

The dependence of light intensity for SLEO *a*-plane GaN, planar *a*- and *c*-plane GaN LEDs on the drive current ($L$–$I$) curve is illustrated in Fig. 5a. The drive current ranged from 20 mA to 1 A, depending on the material quality. Because the device structure and doping levels for this LED set were not optimized, the relative values have more significance than the absolute values.

External quantum efficiency (EQE) is defined as the cross product in between injection efficiency ($\eta_{\text{injection}}$), internal quantum efficiency ($\eta_{\text{internal}}$), and extraction efficiency ($\eta_{\text{extraction}}$), where $\eta_{\text{injection}}$ can be controlled with doping levels and usually regarded as equal to unity. To figure out the internal quantum efficiency, the devices should be packaged and all the light generated should be collected with an integrating sphere or time resolved photolumines-

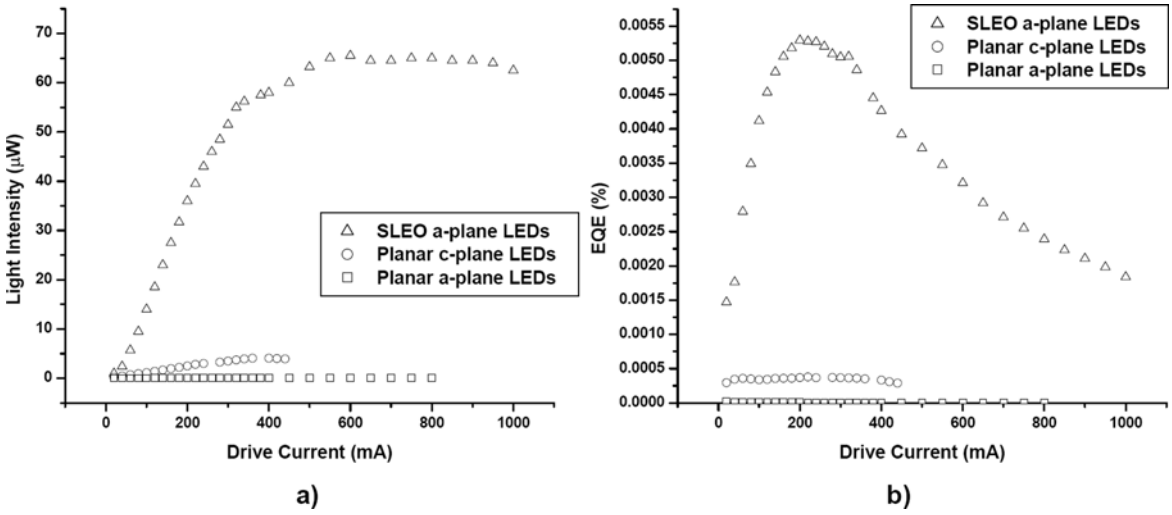


**Figure 5** a) Change in output power, and b) change in external quantum efficiency (EQE) with increase in drive current for on-wafer *a*-plane SLEO, planar *c*-plane, and planar *a*-plane LEDs (400 × 400 μm junction area).

cence experiments should be carried out on the wells. Since the testing was done on an unpackaged wafer, only the EQE was analyzed. For SLEO *a*-plane GaN LEDs the highest EQE was observed as 0.0055% at 200 mA after which the EQE started to decrease gradually with increasing drive current up to roll-off current of 1 A (Fig. 6a). This EQE value is the first reported value for nonpolar *a*-plane UV LEDs. Continuous wave output power as high as 65 μW was measured at 200 mA. The decrease in EQE and saturation of power output were related to heating. Since the internal resistance was relatively lower, longer EQE decay range and the higher roll-off current at 1 A were observed for SLEO LEDs compared with the planar counterparts.

It is shown in Fig. 6c that while planar *a*-plane GaN LEDs output power increases with increasing current, there is no observable peak for EQE due to high internal resistance related with high defect densities. The highest EQE obtained for planar *a*-plane GaN LEDs was 0.00002%, which was almost 275 times lower than what was observed for SLEO LEDs. Considering the fact that both *a*-plane LEDs were free from polarization fields and both of them were grown and processed together, the tremendous amount of difference in EQE could come only from the presence of the defects. By just lowering the defect densities 3–4 orders of magnitude, it was possible to improve device efficiencies in the magnitude of 275×.

The highest EQE obtained for polar planar *c*-plane GaN LEDs was at 200 mA with 0.00038%, which was ~20× higher than planar *a*-plane GaN LEDs and ~15× lower than high quality SLEO LEDs. Although it is not very accurate to compare two different materials that are polar and nonpolar, considering the fact that *c*-plane GaN LEDs had polarization related quantum confined stark effect (QCSE) but relatively lower dislocation densities than nonpolar planar *a*-plane GaN LEDs, the major contributor to 20× difference in EQE was the presence of defects. Also, both SLEO and planar *c*-plane GaN LEDs demonstrated similar trends in device efficiencies. However, *c*-plane GaN LEDs heated at much lower currents and rolled-off at ~400 mA. This also indicates that defect reduction enhances the device lifetime.

Figure 7 demonstrates the effect of contact geometry on the performance of planar *a*-plane GaN LEDs. For all devices due to better current spreading, the Interdigitated (E-shaped) contact geometry devices yielded the best power results. The interdigitated contacts exhibited the highest power output at 0.068 μW and roll-off current at ~400 mA, while for U-shape contacts these values dropped down to 0.059 μW and ~350 mA, respectively. For L-shape contacts the power out and roll-off current were 0.05 μW and ~400 mA, respectively. The higher roll-off currents can be directly attributed to lower device heating due to improved conductivity with better current spreading and lower series resistance. "$P_{\text{without heating}} - P_{\text{with heating}}$" depends on the power dissipation in the device, defined as "$I^2 \times R$" thus the higher the resistance, the higher the power dissipation. Diode, contact and spreading resistance are the major contributors for series resistance. In this case, the material quality is the same and so is the internal resistance. However, since the contact geometry, contact and spreading resistances are different; they contribute differently in series resistance. Also, reduced output power for L-shaped devices can be attributed to a current crowding effect which prevents the uniform illumination throughout the surface.

**4 Conclusion** The two major challenges to improve the device performances can be summarized as eliminating polarization field and related effects, and reducing the defect densities in the material. Both of these challenges have been overcome by growing high quality reduced defect density (TDs of $10^6$–$10^7$ cm$^{-2}$ throughout the material) nonpolar *a*-plane GaN templates using sidewall lateral epi-

 

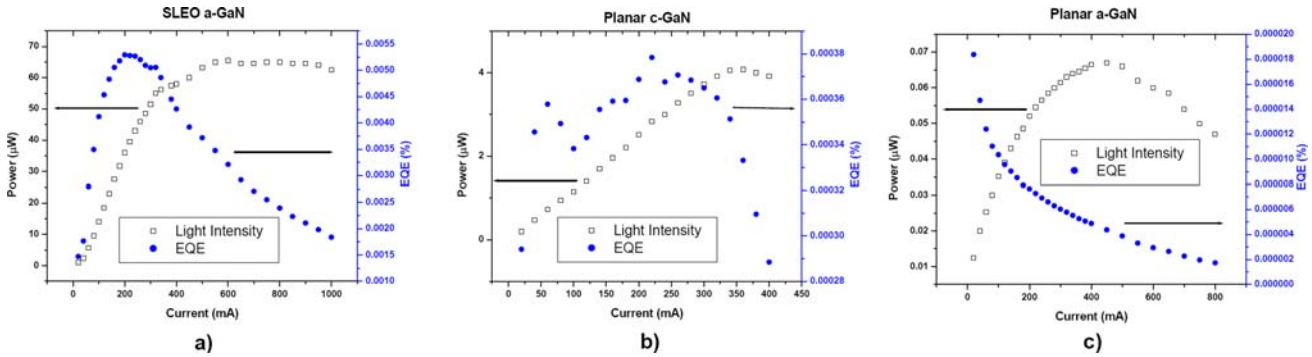


**Figure 6** (online colour at: www.pss-a.com) Change in output power and external quantum efficiency for on-wafer (unpackaged) a) SLEO *a*-plane, b) planar *c*-plane, and c) planar *a*-plane LEDs (400 × 400 μm junction area).

taxial overgrowth (SLEO) method [11]. In this paper, electrical and optical properties of this high quality material were investigated by comparing with the device performances of defected planar *a*-plane (TDs ~$10^{10}$ $cm^{-2}$) and planar *c*-plane LEDs (TDs ~$10^{7}$–$10^{8}$ $cm^{-2}$). To be able to make direct comparison all templates were co-loaded for device growth and processed together. The device structure and doping levels for this LED set were not optimized. Therefore, in some parts of the analysis, relative values had more implication.

Both electrical and optical performances of the devices with lower defect densities improved significantly. The SLEO LEDs exhibited high luminescence intensity (~10–15× higher than planar *c*-plane GaN LEDs) while emission from planar *a*-plane GaN films were extremely weak, therefore the EL emission could not be measured. The EL emission linewidth for SLEO *a*-plane GaN LEDs was 7 nm. For SLEO LEDs the output power at 20 mA drive current was in the range of 2.5–6.5 μW for various types of contact geometries and different test area, for planar *a*-plane GaN films this value was in the range of 0.02–0.05 μW, and for planar *c*-plane GaN films the output power was in the range of 0.3–0.5 μW. The typical series resistance values for SLEO *a*-plane GaN, planar *c*-plane GaN, and planar *a*-plane GaN LEDs were in the range of 15–22 Ω, 28–34 Ω, and 40–45 Ω, respectively, depending on the contact geometry.

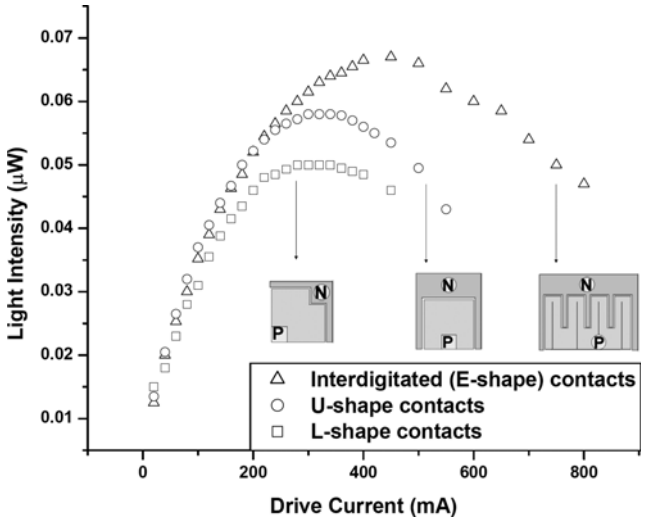


**Figure 7** *L*–*I* characteristics of planar *a*-plane GaN/$Al_{0.15}$GaN unpackaged LEDs for interdigitated (E-shape), U-shape, and L-shape devices with 40 × 400 μm junction area.

With the high quality SLEO material, ~100–300 times higher EQE and ~2.5–3 times lower series resistance values were obtained compared with high defect density planar films. Therefore, effective defect reduction along with elimination of the polarization fields is essential for improving upon the conductivity, doping ionization, electron mobility, radiative recombination, device lifetimes and so ultimately the UV LED performances. In order to realize the true potential of the nonpolar SLEO UV LEDs the device structure, doping levels, and mask design need to be optimized, and for further EQE improvement the extraction efficiency of the devices can be enhanced by packaging, removing the absorbing buffer layers, surface roughening, etc.

The effect of contact geometry was also investigated. The interdigitated (E-shape) contacts yielded the highest output power, lowest series resistance, and the best heat management properties compared with the U- and L-shaped contact geometries due to better current spreading, lower contact resistance, and alleviated current crowding.

**Acknowledgements** The authors would like to acknowledge the support of JST/ERATO and the National Science Foundation for use of Facilities through the MRSEC program.

## References

[1] D. Morita, M. Yamamoto, K. Akaishi, K. Matoba, K. Yasutomo, Y. Kasai, M. Sano, S. Nagahama, and T. Mukai, J. Appl. Phys. **43**, 5945 (2004).
[2] J. Edmond, A. Abare, M. Bergman, J. Bharathan, K. L. Bunker, D. Emerson, K. Haberern, J. Ibbetson, M. Leung, P. Russel, and D. Slater, J. Cryst. Growth **272**, 242 (2004).
[3] J. Deng, Y. Bilenko, A. Lunev, X. Hu, T. M. Katona, J. Zhang, M. S. Shur, and R. Gaska, Jpn. J. Appl. Phys. **46**, L263 (2007).
[4] E. S. Hellman, Z. Liliental-Weber, and D. N. E. Buchanan, MRS Internet J. Nitride Semicond. Res. **2**, 30 (1997).

[5] M. H. Crawford, J. Han, W. W. Chow, M. A. Banas, J. J. Figiel, L. Zhang, and R. J. Shul, Proc. SPIE **3938**, 26 (2000).
[6] A. Chakraborty, B. A. Haskell, S. Keller, J. S. Speck, S. P. DenBaars, S. Nakamura, and U. K. Mishra, Appl. Phys. Lett. **85**, 5143 (2004).
[7] A. Chakraborty, B. A. Haskell, S. Keller, J. S. Speck, S. P. Denbaars, S. Nakamura, U. K. Mishra, Jpn. J. Appl. Phys. **44**, L173 (2005).
[8] M. D. Craven, S. H. Lim, F. Wu, J. S. Speck, and S. P. DenBaars, Appl. Phys. Lett. **81**, 469 (2002).
[9] M. D. Craven, F. Wu, A. Chakraborty, B. Imer, U. K. Mishra, S. P. DenBaars, and J. S. Speck, Appl. Phys. Lett. **84**, 1281 (2004).
[10] C. Chen, V. Adivarahan, J. Yang, M. Shatalov, E. Kuokstis, and M. A. Khan, Jpn. J. Appl. Phys. **42**, L1039 (2003).
[11] B. Imer, F. Wu, S. P. DenBaars, and J. S. Speck, Appl. Phys. Lett. **88**, 061908 (2006).
[12] G. Traetta, A. Di Carlo, A. Reale, P. Lugli, M. Lomascolo, A. Passaseo, R. Cingolani, A. Bonfiglio, M. Berti, E. Napolitani, M. Natali, S. K. Sinha, and A. V. Drigo, J. Cryst. Growth **230**, 492 (2001).
[13] K. C. Zeng, J. Li, J. Y. Lin, and H. X. Jiang, Appl. Phys. Lett. **76**, 3040 (2000).
[14] H. Hirayama and Y. Aoyagi, MRS Internet J. Nitride Semicond. Res. **4S1**, G3.74 (1999).
[15] P. Waltereit, O. Brandt, M. Ramsteiner, R. Uecker, P. Reiche, and K. H. Ploog, J. Cryst. Growth **218**, 143 (2000).
[16] A. Bhattacharyya, I. Friel, S. Iyer, T.-C. Chen, W. Li, J. Cabalu, Y. Fedyunin, K. F. Ludwig Jr., T. D. Moustakas, H.-P. Maruska, D. W. Hill, J. J. Gallagher, M. C. Chou, and B. Chai, J. Cryst. Growth **251**, 487 (2003).
[17] G. A. Garret, H. Shen, M. Wraback, B. Imer, B. Haskell, J. S. Speck, S. Keller, S. Nakamura, and S. P. DenBaars, phys. stat. sol. (a) **202**, 846 (2005).
[18] T. M. Katona, T. Malgalith, C. Moe, M. C. Schmidt, S. Nakamura, J. S. Speck, and S. P. DenBaars, Proc. SPIE **5187**, 250 (2004).
[19] J. J. Wierer, C. Chen, G. Christenson, L. W. Cook, M. G. Craford, A. Edwards, R. M. Fletcher, N. F. Gardner, W. Goetz, W. R. Imler, E. Johnson, R. Kern, R. Khare, F. A. Kish, M. R. Krames, C. Kuo, H. Liu, M. J. Ludowise, R. Mann, M. Maranowski, S. A. Maranowski, P. S. Martin, S. L. Rudaz, D. A. Steigerwald, J. Thompson, J. G. Yu, D. Basile, Y. Chang, M. Heuschen, K. Killeen, C. P. Kocot, S. Rosner, R. P. Schneider, Jr., and T. S. Tan, Proc. SPIE **3938**, 2 (2000).
[20] X. Gao, Y. L. Li, and E. F. Schubert, Appl. Phys. Lett. **79**, 1936 (2001).
[21] T. Mukai and S. Nakamura, Jpn. J. Appl. Phys. **38**, 5735 (1999).

 